Received 9 June 2023; revised 23 July 2023; accepted 31 July 2023. Date of publication 8 August 2023; date of current version 5 September 2023.

Digital Object Identifier 10.1109/OJCOMS.2023.3303248

Interference and Noise Cancellation for Joint Communication Radar (JCR) System Based on Contextual Information

CHRISTANTUS OBINNA NNAMANI [1] (Member, IEEE), AND MATHINI SELLATHURAI [2] (Senior Member, IEEE)

[1]School of Aerospace, Transport and Manufacturing, Cranfield University, MK43 0AL Bedford, U.K.
[2]School of Engineering and Physical Sciences, Heriot-Watt University, EH14 4AS Edinburgh, U.K.

CORRESPONDING AUTHOR: M. SELLATHURAI (e-mail: m.sellathurai@hw.ac.uk)

This work was supported in part by U.K. EPSRC under Grant EP/P009670/1 and Grant EP/T021063/1, and in part by the Petroleum Technology Development Fund under Grant PTDF/ED/PHD/NCO/1352/18.

ABSTRACT This paper examines the separation of wireless communication and radar signals, thereby guaranteeing cohabitation and acting as a panacea to spectrum sensing. First, considering that the channel impulse responses were known by legitimate receivers (communication and radar), we showed that the optimizing beamforming weights mitigate the interference caused by signals and improve the physical layer security (PLS) of the system. Furthermore, when the channel responses were unknown, we designed an interference filter as a low-complex noise and interference cancellation autoencoder. By mitigating the interference on the legitimate users, the PLS was guaranteed. Results showed that even for a low signal-to-noise ratio, the autoencoder produces low root-mean-square error (RMSE) values.

INDEX TERMS Radar, wireless communication, autoencoder, contextual information, joint communication and radar, physical layer security.

I. INTRODUCTION

DUE TO advances in vehicular infrastructure and the need for driverless vehicles, studies into the feasibility of the cohabitation of various sensors operating at diverse spectrum bands began to emerge [1], [2], [3]. This was further exacerbated by the congestion of the below 6GHz spectrum band mainly used for low-earth spectrum applications. A prominent sandwich of application in most discourse is radar and wireless communication (herein referred to as communication) applications with critical reviews presented in [1], [4]. Both spectrums, in principle, can collaborate via cohabitation, co-design and cooperation [4]. However, the collaboration is marred by several design challenges such as interference management, varying power requirements, integration and security. A typical paradigm presents that radar signals require higher transmit power than conventional wireless communication signals. However, the reflected radar signal used in target assessment is considered low-power making it highly susceptible to interference from communication signals. Such an exemplar describes the need for cohabitation for both signals to optimize the usage of the available spectrum.

The cohabitation of radar and communication signals is broadly discussed under the dual-function radar communication (DFRC) and joint communication and radar (JCR) models using multiple input multiple outputs (MIMO) systems. While the latter presents complementary roles for both signals, the former describes a waveform that inseparably represents both signals. Overviews of the coexistence of communication and radar systems were presented in [5, part 1], [6], [7].

A trade-off analysis for the conflicting requirements of power and signal space for a JCR half-duplex system was addressed in [8]. In [5, part 2], a scheme that estimates the communication channel while conducting radar target detection was proposed. The scheme uses a hybrid-analogue-digital (HAD) beamformer to transmit pilot signals for channel estimation and target searching. Similarly, an

interweave full-duplex co-existence scheme was presented in [9], where the radar signal was projected onto the null space of the channel matrix between the radar and communication signals. Soft physical layer security (PLS) guarantees cannot be obtained for the JCR systems due to the exposure of the communication signals to the radar target(s) and receivers. PLS of the cohabitation of radar and communication systems considers that the radar targets and/or receivers may likely be unintended receivers of communication signals to eavesdrop on the transmission.

In the DFRC, embedded communication signals were performed on the beamforming weights and the orthogonal waveform or vice versa [10]. Emphasizing maintaining power levels and maximizing signal-to-interference noise ratio (SINR), the beam pattern obtained from the covariance matrix of the radar signal was used to obtain the transmit beamforming through zero-forcing precoding [11]. Therefore, beamforming designs for full and/or half-duplex transmit and receive communication mitigates the interference between radar and communications signals at the expense of the PLS of the communication signals. However, to ameliorate the PLS concerns, the communication signal and some artificial noise (AN) were embedded into the beamforming weights of the radar transmission [12]. Furthermore, the DFRC system was implemented by using the main lobe for radar and the sidelobes for communication transmissions [13]. The communication signals were embedded in the waveforms determined by 2 different beamforming weights (representing 0 and 1). Although attempts were made by [12] and [13] to incorporate PLS in the DFRC system, they were transmission-centred, based on statistical knowledge of the channel impulse and required handshake between the communication transmitter and genuine receivers.

Nevertheless, if real-time channel information and/or noise impact are unavailable, PLS and interference management challenges become exacerbated. These are further worsened when the establishment of a communication handshake is impossible. Considering the autonomous multi-application domain, it is apparent that the receiver systems become equipped with interference cancellation abilities to maximise the quality of the received signal and improve the PLS of the communication. Therefore, the novel contributions of this paper were to present a technique to perform wireless communication sensing at the legitimate receivers (communication and radar) and to evaluate its impact on PLS for passive eavesdropping. Hence, we outline the main contributions of the paper as:

1) providing receiver-centric wireless sensing capability at the legitimate receivers to enable them to filter the required signal from the sandwiched received signals, and
2) evaluating the possibility of using the interfering radar signals to improve the physical layer security of wireless communication.

The technique discussed herein presented a receiver-based wireless communication approach. We also note that the proposed technique degrades the impact of interference on the received signals. Hence, the objectives of the receiver-based wireless communication sensing technique are enumerated as follows:

1) To separate the wireless communication from its cohabiting radar signals using an interference filter designed as a low-complex noise and interference cancellation autoencoder. This method guaranteed the cohabitation of wireless communication and radar signals and also acts as a panacea for transmit-based spectrum sensing.
2) When the channel impulse response was unknown by the legitimate receivers, to evaluate the performance of the noise and interference cancellation autoencoder on improving PLS.
3) Considering that the channel impulse response was known by the legitimate receivers, to show that optimising beamforming weights mitigate the interference caused by signals and improve the PLS of the system.

To achieve these objectives, we first evaluate the performance of the communication and radar cohabiting system when its design allows for the cancellation of the interfering signals to both receivers. This was achieved by assuming the channel information is available and nulling the interfering transmissions with beamforming weights. Furthermore, relaxing the assumption on the channel information (i.e., by considering that the channel information is unknown), this paper proposes an interference mitigation scheme implemented with autoencoders. We focus on separating transmitted communication and radar signals at the receiver of the communication and the radar system using novel noise and interference cancellation filters. Our novel approach entails the use of autoencoders at the receivers to filter out the interfering and noise signals. We note that the proposed method curtails the requirement for spectrum sensing since the impact of the interfering signal is minimized in terms of SINR. By limiting the spurious interfering communication signal impinging on the legitimate receivers while confusing the eavesdroppers, PLS performance was improved. Similarly, by reducing the radar interference, the communication transmission rate was also improved.

In practice, an application of the proposed noise and interference cancellation filter aids autonomous vehicular radar's impact on wireless communication infrastructure. Although it minimizes the impact of the DFRC and/or JCR constraints, we focus on the cohabiting of the JCR system without loss of generalization. We emphasize that the overall objective entails the cancellation of interference at legitimate receivers based on previously acquired contextual information of the system's reaction to cohabitation. Such contextual information as applicable to radar tracking systems using neural networks [14] were implemented. Specifically, the contextual information is obtained from an

a priori knowledge of observations of the JCR system with pilot/test sample signals.

Notations: The structure of the notations employed in this paper elucidates that $\{\cdot\}^*$, $\{\cdot\}^{\mathrm{T}}$ and $\{\cdot\}^{\mathrm{H}}$ represent the conjugate, transpose and Hermitian of vectors/matrices, respectively. Low case letters are scalars, bold-faced low case letters are vectors while bold-faced upper case letters are matrices. Furthermore, rank($\mathbf{X}$) and Tr($\mathbf{X}$) are the rank and trace of matrix $\mathbf{X}$ respectively. Furthermore, the operator, $|.|$ is a norm operator which can be expressed as the square root of the inner product of the vector $|\mathbf{x}| = \sqrt{\mathbf{x}^{\mathrm{H}}\mathbf{x}}$ while $\nabla^2 f$ is the Hessian or second derivative of a function, f.

II. SYSTEM MODEL OF A COMMUNICATION/RADAR COHABITING SCENARIO

Consider a MIMO communication system with N_{A} transmit and N_{B} receive antennas operating at the radar spectrum. Let the communication system cohabit with MIMO radar systems with N_{D} transmit and N_{C} receive antennas. For computational simplicity, we assume that the transmit and receive radar systems are located at the same place such that they share the same far-field observations. However, the assumption does not necessarily apply to the communication system, thereby supporting their joint action. The $N_{\mathrm{D}} \times 1$ and $N_{\mathrm{A}} \times 1$ passband signals of the radar and communication transmit antennas are presented in (1a) and (1b) respectively.

$$\mathbf{s}_m(t) = \mathbf{w}_m^* \psi_m(t), \ \forall\ m = \{1, \ldots, M\} \tag{1a}$$

$$\mathbf{s}_{\mathrm{AB}}(t) = \mathbf{w}_{\mathrm{AB}}^* \varphi(t), \ \forall\ t = \{1, \ldots, T\}. \tag{1b}$$

where $\mathbf{w}_k$ represent the $N_{\mathrm{D}} \times 1$ transmit beamforming vector of the mth orthogonal waveform ($\psi_m(t)$). $\mathbf{w}_{\mathrm{AB}}$ the $N_{\mathrm{A}} \times 1$ is the transmit weight vector of the communication systems. M is the total number of orthogonal waveforms radiated by the radar system (for simplicity, $M = N_{\mathrm{D}}$ implying that the radar transmission is orthogonal for each antenna) and T is the total number of transmit snapshots. While $\varphi(t)$ is the baseband communication signal waveform. If we assume frequency hopping communication transmission with quadrature phase shift keying (PSK) modulation, then $\varphi(t)$ is presented in [10, eq. (9)]. In the rest of this paper, the subscripts A, B, C, D, E denote an index of the communication transmitter, communication legitimate receiver (Bob), radar transmitter, radar receiver and communication illegitimate receiver (Eve) respectively. We note that in the context of JCR, the communication and radar transmit systems are usually co-located, sharing the same physical resources. However, spatial separation has been introduced in Fig. 1 for clarity.

To understand the operational requirements of the entire system model, we discuss 2 distinct roles of the radar system in relation to the communication system. The distinct roles are considered when the radar target is absent and when it is present.

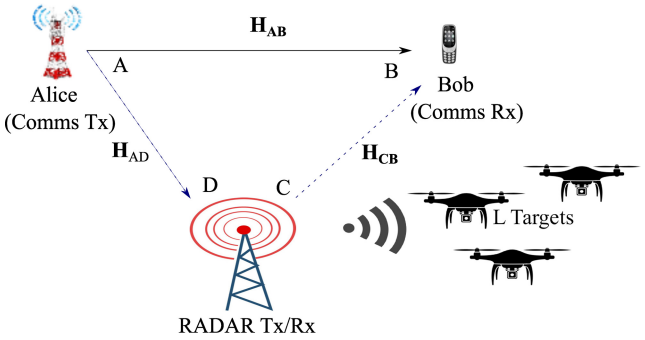

FIGURE 1. MIMO communication and radar cohabitation system.

A. CASE 1

In this section, we model the received signals of the communications and radar receiver systems under JCR when they are no radar targets. The received signal at the communication and the radar receivers are given as (2a) and (2b) respectively.

$$\mathbf{y}_i(t) = \underbrace{\mathbf{H}_{\mathrm{A}i}\mathbf{s}_{\mathrm{AB}}(t)}_{\text{Comms. transmitted}} + \underbrace{\mathbf{H}_{\mathrm{C}i}\mathbf{s}_m(t)}_{\text{radar interfered}} + \mathbf{n}_i, \tag{2a}$$

$$\mathbf{y}_{\mathrm{D}}(t) = \underbrace{\mathbf{H}_{\mathrm{AD}}\mathbf{s}_{\mathrm{AB}}(t)}_{\text{Comms. transmitted}} + \mathbf{n}_{\mathrm{D}}, \tag{2b}$$

$\forall\ i \in \{\mathrm{B,E}\}$, and where $\mathbf{H}_{\mathrm{A}i} = \mathbf{b}(\theta_{i\mathrm{A}})\alpha_{\mathrm{A}i}\mathbf{a}^{\mathrm{T}}(\theta_{\mathrm{AB}})$, $\mathbf{H}_{\mathrm{AD}} = \mathbf{d}(\theta_{\mathrm{DA}})\alpha_{\mathrm{AD}}\mathbf{a}^{\mathrm{T}}(\theta_{\mathrm{AB}})$, $\mathbf{H}_{\mathrm{C}i} = \mathbf{b}(\theta_{i\mathrm{C}})\alpha_{\mathrm{C}i}\mathbf{c}^{\mathrm{T}}(\theta)$. $\alpha_{jk} = \rho_0\zeta\|\boldsymbol{\Omega}_j - \boldsymbol{\Omega}_k\|^{-2}$, $\forall\ \{j\ \&\ k \in \{\mathrm{A,B,C,D,E}\}\}$ are random channel coefficients characterizing the propagation from path j to k. ρ_0 represents the channel power gain at reference distance $d_0 = 1$ m and ζ is an exponential random variable with unit mean similar to [15], [16], [17]. Parameters $\mathbf{a}(\theta_{\mathrm{AB}})$ and $\mathbf{c}(\theta)$ are the transmit communication and radar steering vectors respectively. While $\mathbf{b}(\theta_{i\mathrm{A}})$, $\mathbf{b}(\theta_{i\mathrm{C}})$ and $\mathbf{d}(\theta_{\mathrm{DA}})$ are the receive steering vectors for the communication and radar systems. Note that the communication receivers include the legitimate receiver (Bob) and the eavesdropper (Eve) as required. Assume that the antenna geometry on the communication and radar systems follow a uniform linear array (ULA) configuration, then the steering vectors were generated with

$$\mathbf{x}(\theta_{jk}) = [1, e^{j\frac{2\pi}{\lambda}d_x \sin(\theta_{jk})}, \ldots, e^{j\frac{2\pi}{\lambda}(N_i-1)d_x \sin(\theta_{jk})}]^{\mathrm{T}},$$

where d_x is the distance between antenna elements. Furthermore, $\mathbf{n}_{\mathrm{B}} \sim \mathcal{CN}(0, \sigma_{\mathrm{B}}^2\mathbf{1}_{N_{\mathrm{B}}})$ and $\mathbf{n}_{\mathrm{D}} \sim \mathcal{CN}(0, \sigma_{\mathrm{D}}^2\mathbf{1}_{N_{\mathrm{C}}})$ are additive white Gaussian noise with variance σ_{B}^2 and σ_{D}^2. The spatial direction of the radar system is focused towards a predefined sector such that $\theta = [\Theta_{\min}, \Theta_{\max}]$ where $\Theta_{\min}$ and $\Theta_{\max}$ represents the lower and upper contours of the sector. We note that θ_{jk} is the azimuth spatial direction of transmission from the j to the k or reception at j from k.

B. CASE 2

Consider Fig. 1 where hypothetical L radar targets reflect radar signals. The received signal equations at the communication and radar receiver are given in (3a) and (3b)

respectively.

$$\mathbf{y}_i(t) = \mathbf{H}_{\mathrm{A}i}\mathbf{s}_{\mathrm{AB}}(t) + \mathbf{H}_{\mathrm{C}i}\mathbf{s}_m(t) + \underbrace{\sum_{l=1}^{L}\mathbf{H}_{li}\mathbf{s}_m(t)}_{\text{target reflected}} + \mathbf{n}_i, \quad (3a)$$

$$\mathbf{y}_{\mathrm{D}}(t) = \mathbf{H}_{\mathrm{AD}}\mathbf{s}_{\mathrm{AB}}(t) + \underbrace{\sum_{l=1}^{L}\mathbf{H}_{l\mathrm{D}}\mathbf{s}_m(t)}_{\text{target reflected}} + \mathbf{n}_{\mathrm{D}}, \quad (3b)$$

$\forall\, i \in \{\mathrm{B},\mathrm{E}\}$, and where $\mathbf{H}_{li} = \mathbf{b}(\theta_{il})\alpha_{li}\beta_l\alpha_{lr}\mathbf{c}^{\mathrm{T}}(\theta)$, $\mathbf{H}_{l\mathrm{D}} = \mathbf{d}(\theta_{\mathrm{D}l})\alpha_{l\mathrm{D}}\beta_l\alpha_{lr}\mathbf{c}^{\mathrm{T}}(\theta)$. β_l obeys the Swerling II model and represents the reflection coefficient of the lth target. The Swerling II model implies that the reflectivity of the target will change for a different pulse, but it will be constant within the duration of a single pulse duration.

Section summary: In the cases described in Sections II-A and II-B, it is underlined that some form of cross-interference exists for the communication and radar systems especially when their channels are correlated. For the communication signal containing relevant data, its interference on the radar receiver makes it susceptible to eavesdropping. By mitigating the interference, the loss of data in the physical layer domain is reduced.

III. INTERFERENCE MITIGATION

In this section, we examine the methods to mitigate the interference caused by the communication transmission on the radar reception and vice versa. The interference mitigation approaches are discussed under two distinct generic scenarios, namely cooperative and uncooperative systems. The scenarios characterise the arguments described in the paper. The first argument of the paper presents that when the channel responses are known by the transmitter and legitimate receivers (cooperative), the signal can be targeted to the legitimate receiver by designing the beamformer to propagate on the channel of the legitimate receiver while nulling the interference caused to the other transmitter (wireless communication or radar). The design of the beamformer depends on the knowledge of the channel impulse response. The second argument is that when the channel responses are unknown (uncooperative), then we proposed a receiver autoencoder-based filter that was designed in the context of historic transmission.

A. COOPERATIVE SYSTEMS

The radar and communication systems are cooperative when the channel impulse responses between the transmitters and receivers are known by both systems. This entails that channel estimation had been carried out and updated in both systems. Using this contextual information of the *a priori* channel information, the interfering signals are reduced in the transmitter design. It is easy to see that interference cancellation is obtained by independently optimizing the transmit beamforming weights of both the communication and radar transmissions, in the case discussed in Section II-A. However, the design of the beamforming weights does not cancel the interference caused by radar target reflection as in the case discussed in Section II-B. To buttress the theoretical formulation, we formulate the optimization problems in (4) and (7) to design the beamformer for communication and radar systems respectively. We note that both equations were independently solved at the communication and radar transmitters.

1) COMMUNICATION BEAMFORMER

The problem formulated in this section defines the beamforming weights that will be applied to the communication transmitter to ensure minimum interference on the radar and maximum communication reception.

$$\max_{\mathbf{w}_{\mathrm{AB}}} \quad \log_2\left(1+\gamma_{\mathrm{B}}\right), \quad (4a)$$

$$\text{s.t.} \quad |\mathbf{H}_{\mathrm{AD}}\mathbf{s}_{\mathrm{AB}}(t)|^2 = 0, \quad (4b)$$

$$\mathbf{w}_{\mathrm{AB}}^{\mathrm{H}}\mathbf{w}_{\mathrm{AB}} = 1, \quad (4c)$$

where γ_{B} represents the SINR at the legitimate receiver (Bob) are its expression given in (5). The objective of (4) was to design the communication beamforming weights such that the communication signal is transmitted with the optimal rate to the intended receiver (refer to (4a)). At the same time, the design of the beamforming weights of the communication signals also ensures that the communication signal does not interfere with the radar receiver. Hence, the constraint in (4b) ensures the channel between the communication transmitter and the radar receiver is nulled by the design of the beamforming weights. By nulling the channel, we design communication beamforming weights that sum to zero at the radar receiver thereby, reducing interference.

$$\gamma_{\mathrm{B}} = \frac{|\mathbf{H}_{\mathrm{AB}}\mathbf{s}_{\mathrm{AB}}(t)|^2}{\sum_{l=1}^{L}|\mathbf{H}_{l\mathrm{B}}\mathbf{s}_m(t)|^2 + |\mathbf{H}_{\mathrm{CB}}\mathbf{s}_m(t)|^2 + \sigma_{\mathrm{B}}^2}. \quad (5)$$

Equation (5) provides the SINR at the legitimate receiver (Bob). The numerator of (5) depicts the received signal power while the denominator contains the interfering signals from the reflected and the source radar signals.

We note that the norm operator $|.|$, can be transformed using the relation, $|\mathbf{H}\mathbf{x}|^2 = \mathrm{Tr}(\mathbf{H}\mathbf{x}\mathbf{x}^{\mathrm{H}}\mathbf{H}^{\mathrm{H}})$. The proof of the transformation can be obtained following from the definition of the norm operator given as $|\mathbf{x}| = \sqrt{\mathbf{x}^{\mathrm{H}}\mathbf{x}}$. Therefore $|\mathbf{H}\mathbf{x}|^2 = (\mathbf{H}\mathbf{x})^{\mathrm{H}}\mathbf{H}\mathbf{x}$. By applying [18, eq. (9) and (17)], we have $(\mathbf{H}\mathbf{x})^{\mathrm{H}}\mathbf{H}\mathbf{x} = \mathbf{x}^{\mathrm{H}}\mathbf{H}^{\mathrm{H}}\mathbf{H}\mathbf{x}$ and $\mathbf{x}^{\mathrm{H}}\mathbf{H}^{\mathrm{H}}\mathbf{H}\mathbf{x} = \mathrm{Tr}(\mathbf{H}\mathbf{x}\mathbf{x}^{\mathrm{H}}\mathbf{H}^{\mathrm{H}})$ respectively.

By applying the transformation to the norm operators and substituting for $s_{\mathrm{AB}}(t)$ and $s_m(t)$, the problem in (4) can be re-written as (6).

$$\max_{\mathbf{W}_{\mathrm{AB}}} \quad \log_2\left(1+\gamma_{\mathrm{B}}\right), \quad (6a)$$

$$\text{s.t.} \quad \mathrm{Tr}(\mathbf{H}_{\mathrm{AD}}\mathbf{W}_{\mathrm{AB}}\mathbf{H}_{\mathrm{AD}}^{\mathrm{H}}) = 0, \quad (6b)$$

$$\mathrm{Tr}(\mathbf{W}_{\mathrm{AB}}) = 1, \quad (6c)$$

where $\mathbf{W}_{\mathrm{AB}} = \mathbf{w}_{\mathrm{AB}}\mathbf{w}_{\mathrm{AB}}^{\mathrm{H}}$. The solution of $\mathbf{w}_{\mathrm{AB}}$ can be obtained from $\mathbf{W}_{\mathrm{AB}}$ using randomisation. Also, γ_{B} presented in (5) was expanded to $\gamma_{\mathrm{B}} = \frac{\mathrm{Tr}(\mathbf{H}_{\mathrm{AB}}\mathbf{W}_{\mathrm{AB}}\mathbf{H}_{\mathrm{AB}}^{\mathrm{H}})}{\sum_{l=1}^{L}\mathrm{Tr}(\mathbf{H}_{l\mathrm{B}}\mathbf{W}_k\mathbf{H}_{l\mathrm{B}}^{\mathrm{H}})+\mathrm{Tr}(\mathbf{H}_{\mathrm{CB}}\mathbf{W}_k\mathbf{H}_{\mathrm{CB}}^{\mathrm{H}})+\sigma_{\mathrm{B}}^2}$.

2) RADAR BEAMFORMER

The emphasis of the problem formulated in this section is on the transmit beamforming weights of the radar transmitter. The objective is to design the beamforming weights of the radar transmitter to focus on the target. However, we constrained the beamformer in (7b) to cause minimum interference at the communication receiver.

$$\max_{\mathbf{w}_k} \quad \log_2\left(1+\frac{\sum_{l=1}^{L}|\mathbf{H}_{l\mathrm{D}}\mathbf{s}_m(t)|^2}{|\mathbf{H}_{\mathrm{AD}}\mathbf{s}_{\mathrm{AB}}(t)|^2+\sigma_{\mathrm{D}}^2}\right), \tag{7a}$$

$$\text{s.t.} \quad \sum_{l=1}^{L}|\mathbf{H}_{l\mathrm{B}}\mathbf{s}_m(t)|^2+|\mathbf{H}_{\mathrm{CB}}\mathbf{s}_m(t)|^2=0, \tag{7b}$$

$$\mathbf{w}_k^{\mathrm{H}}\mathbf{w}_k=1. \tag{7c}$$

Using a similar transformation of the norm operator, $|.|$ described in Section III-A1, (7) can be re-written as (8) for $\mathbf{W}_k = \mathbf{w}_k\mathbf{w}_k^{\mathrm{H}}$.

$$\max_{\mathbf{W}_k} \quad \log_2\left(1+\frac{\sum_{l=1}^{L}\mathrm{Tr}(\mathbf{H}_{l\mathrm{D}}\mathbf{W}_k\mathbf{H}_{l\mathrm{D}}^{\mathrm{H}})}{\mathrm{Tr}(\mathbf{H}_{\mathrm{AD}}\mathbf{W}_{\mathrm{AB}}\mathbf{H}_{\mathrm{AD}}^{\mathrm{H}})+\sigma_{\mathrm{D}}^2}\right), \tag{8a}$$

$$\text{s.t.} \quad \sum_{l=1}^{L}\mathrm{Tr}(\mathbf{H}_{l\mathrm{B}}\mathbf{W}_k\mathbf{H}_{l\mathrm{B}}^{\mathrm{H}})+\mathrm{Tr}(\mathbf{H}_{\mathrm{CB}}\mathbf{W}_k\mathbf{H}_{\mathrm{CB}}^{\mathrm{H}})=0, \tag{8b}$$

$$\mathrm{Tr}(\mathbf{W}_k)=1. \tag{8c}$$

3) OVERALL SOLUTION

Following the second derivative convex check method, it can be observed that the objective functions in (6a) and (8a) are concave functions with respect to the optimisation variables $\mathbf{W}_{\mathrm{AB}}$ and $\mathbf{W}_k$.

Given that

$$f(\mathbf{X}) = \log_2\left(1+\frac{\mathrm{Tr}(\mathbf{X}\mathbf{A})}{b}\right),$$
$$\nabla^2 f(\mathbf{X}) = -\frac{(\mathbf{A}^{\mathrm{H}})^2}{(\mathrm{Tr}(\mathbf{X}\mathbf{A})+b)^2}.$$

The concavity of $f(\mathbf{X})$ arises from $\mathbf{v}^{\mathrm{T}}\nabla^2 f(\mathbf{X})\mathbf{v} \le 0$ for all vectors, $\mathbf{v}$ by applying Cauchy-Schwarz inequality. At the same time, all the constraints are affine functions. Therefore, the solutions to (6) and (8) are easily obtained using any convex solvers like CVX [19]. We note that (6c) and (8c) describe the total power transmitted by the communication and radar transmitter respectively. These powers can be scaled to desired level in practice. For $L = 0$, no target reflects the radar signal and the solution is produced for Section II-A.

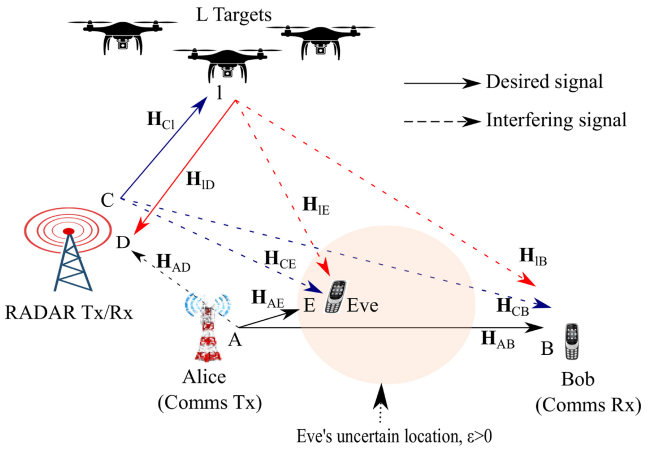

FIGURE 2. MIMO communication and radar cohabitation system with interaction from a passive eavesdropper.

B. PLS ANALYSIS OF THE COMMUNICATION/RADAR COHABITING SCENARIO

Consider that an eavesdropper lurks within the radio vicinity of the wireless communication signal, thereby receiving the legitimate communication transmission and interference generated by the cohabiting transmission (radar). In this section, the characterization of the PLS with communication sensing was performed. The generic cohabitation figure presented in Fig. 1 was expanded in Fig. 2 with the depiction of the passive eavesdropper location to allow for PLS analysis.

Since the eavesdropper is passive, its exact location or signal signature is unknown. However, for simplicity, we assume that it is located within a circular region that spans the coverage area of the transmitters. Therefore, following the derivations in [20], the exact location of Eve ($\mathbf{\Omega}_{\mathrm{E}}$) was defined as a point on a circular uncertain region with uncertainty given in (9).

$$\mathbf{\Omega}_{\mathrm{E}} = \hat{\mathbf{\Omega}}_{\mathrm{E}} \pm \Delta\mathbf{\Omega}_{\mathrm{E}}, \tag{9a}$$

$$\|\pm\Delta\mathbf{\Omega}_{\mathrm{E}}\| = \|\mathbf{\Omega}_{\mathrm{E}} - \hat{\mathbf{\Omega}}_{\mathrm{E}}\| \le \varepsilon, \ \text{for } \varepsilon \ge 0, \tag{9b}$$

$$\|\Delta\mathbf{\Omega}_{\mathrm{E}}\| \le \varepsilon, \tag{9c}$$

holds true, where $\hat{\mathbf{\Omega}}_{\mathrm{E}}$, $\Delta\mathbf{\Omega}_{\mathrm{E}}$ and ε define the estimated location of Eve, the error of the estimation and the radius of error, respectively. The estimated location of Eve influences its channel coefficient previously defined as $\alpha_{j\mathrm{E}} = \rho_0\zeta\|\mathbf{\Omega}_j - \mathbf{\Omega}_{\mathrm{E}}\|^{-2}$, where $j \in \{\mathrm{A,C,l}\}$. Using triangular inequality and substituting (9), we have that

$$\|\mathbf{\Omega}_j - \mathbf{\Omega}_{\mathrm{E}}\| = \|\mathbf{\Omega}_j - (\hat{\mathbf{\Omega}}_{\mathrm{E}} \pm \Delta\mathbf{\Omega}_{\mathrm{E}})\| \le \|\mathbf{\Omega}_j - \hat{\mathbf{\Omega}}_{\mathrm{E}}\| + \varepsilon. \tag{10}$$

The right-hand side is an upper bound to Euclidean distance between the transmitters (communication, radar) and the centre of the circular uncertain region. By substituting the approximation of the upper bound of the location of Eve, we obtain that $\hat{\alpha}_{j\mathrm{E}} = \rho_0\zeta(\|\mathbf{\Omega}_j - \hat{\mathbf{\Omega}}_{\mathrm{E}}\| + \varepsilon)^{-2}$. Hence the SINR of Eve was presented in (11) respectively.

$$\hat{\gamma}_{\mathrm{E}} = \frac{|\mathbf{H}_{\mathrm{AE}}\mathbf{s}_{\mathrm{AB}}(t)|^2}{\sum_{l=1}^{L}|\mathbf{H}_{l\mathrm{E}}\mathbf{s}_m(t)|^2+|\mathbf{H}_{\mathrm{CE}}\mathbf{s}_m(t)|^2+\sigma_{\mathrm{E}}^2}, \tag{11}$$

where $\mathbf{H}_{\mathrm{AE}} = \mathbf{b}(\theta_{\mathrm{EA}})\hat{\alpha}_{\mathrm{AE}}\mathbf{a}^{\mathrm{T}}(\theta_{\mathrm{AB}})$, $\mathbf{H}_{l\mathrm{E}} = \mathbf{b}(\theta_{\mathrm{E}l})\alpha_{l\mathrm{E}}\beta_l\hat{\alpha}_{lr}\mathbf{c}^{\mathrm{T}}(\theta)$. Therefore, similar to assertions in [15], [21], the average secrecy rate given in (13a) is the difference in the information rate of Bob and Eve.

$$R_s = \left[\log_2(1+\gamma_{\mathrm{B}}) - \log_2(1+\hat{\gamma}_{\mathrm{E}})\right]^+, \tag{12}$$

where $[x]^+ = \max\{0, x\}$ ensures that the information rate received by Eve is not greater than that received by Bob, therefore guaranteeing positive average secrecy rates [21], [22]. However, for ease of computation, this constraint on the average secrecy rate is ignored. This was justified by the analysis that the system provides for degrading the eavesdropper's channel leading to positive secrecy rates.

$$\max_{\mathbf{w}_{\mathrm{AB}},\mathbf{w}_k} \quad R_s, \tag{13a}$$

$$\text{s.t.} \quad \log_2\left(1+\frac{\sum_{l=1}^{L}|\mathbf{H}_{l\mathrm{D}}\mathbf{s}_m(t)|^2}{\sigma_{\mathrm{D}}^2}\right) \geq r_{\mathrm{th}}, \tag{13b}$$

$$|\mathbf{H}_{\mathrm{AD}}\mathbf{s}_{\mathrm{AB}}(t)|^2 = 0, \tag{13c}$$

$$\sum_{l=1}^{L}|\mathbf{H}_{l\mathrm{B}}\mathbf{s}_m(t)|^2 + |\mathbf{H}_{\mathrm{CB}}\mathbf{s}_m(t)|^2 = 0, \tag{13d}$$

$$\mathbf{w}_{\mathrm{AB}}^{\mathrm{H}}\mathbf{w}_{\mathrm{AB}} = 1, \tag{13e}$$

$$\mathbf{w}_k^{\mathrm{H}}\mathbf{w}_k = 1. \tag{13f}$$

The parameter r_{th} is the maximum radar rate required to reformulate the reflected signal from the radar targets. Equation (13b) provides the lower bound to the rate received by the radar receiver to reconstruct the reflected signal. Equation (13d) used the known channel information to cancel the interference at the legitimate receiver while (13c) removes the interference of the communication signal at the radar receiver. By substituting for $\mathbf{s}_{\mathrm{AB}}$ and $\mathbf{s}_{\mathrm{AB}}$ with (1b) and (1a) respectively and expanding the objective function, (13) is rewritten as (14).

$$\max_{\mathbf{W}_{\mathrm{AB}},\mathbf{W}_k} \quad \log_2\left(1+\gamma_{\mathrm{B}}\right) - \log_2\left(1+\hat{\gamma}_{\mathrm{E}}\right), \tag{14a}$$

$$\text{s.t.} \quad \log_2\left(1+\frac{\sum_{l=1}^{L}\mathrm{Tr}(\mathbf{H}_{l\mathrm{D}}\mathbf{W}_k\mathbf{H}_{l\mathrm{D}}^{\mathrm{H}})}{\sigma_{\mathrm{D}}^2}\right) \geq r_{\mathrm{th}}, \tag{14b}$$

$$\mathrm{Tr}(\mathbf{H}_{\mathrm{AD}}\mathbf{W}_{\mathrm{AB}}\mathbf{H}_{\mathrm{AD}}^{\mathrm{H}}) = 0, \tag{14c}$$

$$\sum_{l=1}^{L}\mathrm{Tr}(\mathbf{H}_{l\mathrm{B}}\mathbf{W}_k\mathbf{H}_{l\mathrm{B}}^{\mathrm{H}}) + \mathrm{Tr}(\mathbf{H}_{\mathrm{CB}}\mathbf{W}_k\mathbf{H}_{\mathrm{CB}}^{\mathrm{H}}) = 0, \tag{14d}$$

$$\mathrm{Tr}(\mathbf{W}_{\mathrm{AB}}) = 1, \tag{14e}$$

$$\mathrm{Tr}(\mathbf{W}_k) = 1, \tag{14f}$$

$$\mathrm{rank}(\mathbf{W}_{\mathrm{AB}}) = 1, \tag{14g}$$

$$\mathrm{rank}(\mathbf{W}_k) = 1. \tag{14h}$$

Equations (14g) and (14h) were consequences of $\mathbf{W}_{\mathrm{AB}} = \mathbf{w}_{\mathrm{AB}}\mathbf{w}_{\mathrm{AB}}^{\mathrm{H}}$, and $\mathbf{W}_k = \mathbf{w}_k\mathbf{w}_k^{\mathrm{H}}$. We recall that the norm operator $|.|$, were transformed using the relation, $|\mathbf{H}\mathbf{x}|^2 = \mathrm{Tr}(\mathbf{H}\mathbf{x}\mathbf{x}^{\mathrm{H}}\mathbf{H}^{\mathrm{H}})$. Furthermore, the SINR equation given in (5), with the interference nulling performed in (14d), and the SINR of (11) were expanded to

$$\gamma_{\mathrm{B}} = \frac{\mathrm{Tr}\left(\mathbf{H}_{\mathrm{AB}}\mathbf{W}_{\mathrm{AB}}\mathbf{H}_{\mathrm{AB}}^{\mathrm{H}}\right)}{\sigma_{\mathrm{B}}^2}.$$

$$\hat{\gamma}_{\mathrm{E}} = \frac{\mathrm{Tr}\left(\mathbf{H}_{\mathrm{AE}}\mathbf{W}_{\mathrm{AB}}\mathbf{H}_{\mathrm{AE}}^{\mathrm{H}}\right)}{\sum_{l=1}^{L}\mathrm{Tr}\left(\mathbf{H}_{l\mathrm{E}}\mathbf{W}_k\mathbf{H}_{l\mathrm{E}}^{\mathrm{H}}\right) + \mathrm{Tr}\left(\mathbf{H}_{\mathrm{CE}}\mathbf{W}_k\mathbf{H}_{\mathrm{CE}}^{\mathrm{H}}\right) + \sigma_{\mathrm{E}}^2}.$$

We note that (14) is non-convex due to the non-convexity of the objective function. However, it was solved by applying successive convex approximation (SCA). The SCA allows the problem to be broken into sub-optimal problems and iterative algorithms developed to minimize the error of the objective function given in (14a) at each iteration step. The sub-problems and solutions arising from (14) were presented as (15) and (17) and the iterative algorithm was summarized in Algorithm 1.

Algorithm 1 SCA Iterative Algorithm for Solving W_{AB} and W_k

1: Initialize W_{AB}^0, W_k^0 and R_s^0 such that the constraints in (14) were satisfied.
2: $m \leftarrow 1$.
3: **repeat**
4: Compute and update W_{AB}^m with (16).
5: Using updated W_{AB}^m, compute and update W_k^m with (18).
6: Compute R_s^m as defined in (12).
7: $\epsilon = \left|\frac{R_s^m - R_s^{m-1}}{R_s^m}\right|$.
8: $m \leftarrow m+1$.
9: **until** $\epsilon \leq 10^{-5}$ OR $m \geq m_{max}$.
10: **Output:** $W_{\mathrm{AB}} = W_{\mathrm{AB}}^m$ and $W_k = W_k^m$.

First, we present the sub-problem from (14) that solves for the beamforming weights parameter arising from the wireless communication transmission in (15).

$$\max_{\mathbf{W}_{\mathrm{AB}}} \quad \log_2\left(1+\bar{k}_1\mathrm{Tr}\left(\mathbf{H}_{\mathrm{AB}}\mathbf{W}_{\mathrm{AB}}\mathbf{H}_{\mathrm{AB}}^{\mathrm{H}}\right)\right) - \log_2\left(1+\bar{k}_2\mathrm{Tr}\left(\mathbf{H}_{\mathrm{AE}}\mathbf{W}_{\mathrm{AB}}\mathbf{H}_{\mathrm{AE}}^{\mathrm{H}}\right)\right), \tag{15a}$$

$$\text{s.t.} \quad \mathrm{Tr}\left(\mathbf{H}_{\mathrm{AD}}\mathbf{W}_{\mathrm{AB}}\mathbf{H}_{\mathrm{AD}}^{\mathrm{H}}\right) = 0, \tag{15b}$$

$$\mathrm{Tr}(\mathbf{W}_{\mathrm{AB}}) = 1, \tag{15c}$$

$$\mathrm{rank}(\mathbf{W}_{\mathrm{AB}}) = 1, \tag{15d}$$

where $\bar{k}_1 = \frac{1}{\sigma_{\mathrm{B}}^2}$ and

$\bar{k}_2 = (\sum_{l=1}^{L}\mathrm{Tr}(\mathbf{H}_{l\mathrm{E}}\mathbf{W}_k\mathbf{H}_{l\mathrm{E}}^{\mathrm{H}}) + \mathrm{Tr}(\mathbf{H}_{\mathrm{CE}}\mathbf{W}_k\mathbf{H}_{\mathrm{CE}}^{\mathrm{H}}) + \sigma_{\mathrm{E}}^2)^{-1}$.

Equation (15) is a semi-definite programming (SDP) problem which was solved following the conventional approach of neglecting the rank constraint in (15d). Hence, by applying logarithm law, and rewriting the trace matrix with [18, eq. (16)], the objective of (15) was written as fractional objective. Thereby enabling the use of Charnes-Cooper's transformation of the problem to (16). Let $u = (1+\mathrm{Tr}(\mathbf{H}_{\mathrm{AE}}^{\mathrm{H}}\mathbf{H}_{\mathrm{AE}}\mathbf{W}_{\mathrm{AB}}))^{-1}$, and $\mathbf{U} = u\mathbf{W}_{\mathrm{AB}}$, then (15)

is equivalent to (16).

$$\max_{\mathbf{U},u} \quad \left(u + \mathrm{Tr}\left(\bar{k}_1 \mathbf{H}_{\mathrm{AB}}^{\mathrm{H}} \mathbf{H}_{\mathrm{AB}} \mathbf{U}\right)\right), \tag{16a}$$

$$\text{s.t.} \quad \left(u + \bar{k}_1 \mathrm{Tr}\left(\bar{k}_2 \mathbf{H}_{\mathrm{AE}}^{\mathrm{H}} \mathbf{H}_{\mathrm{AE}} \mathbf{U}\right)\right) = 1, \tag{16b}$$

$$\mathrm{Tr}\left(\bar{k}_2 \mathbf{H}_{\mathrm{AD}}^{\mathrm{H}} \mathbf{H}_{\mathrm{AD}} u \mathbf{U}\right) = 0, \tag{16c}$$

$$\mathrm{Tr}(\mathbf{U}) = 1. \tag{16d}$$

Equation (16) is convex and is easily solved with CVX [23]. We note that the rank constraint is dropped in (16) to allow for an SDP solution. However, when the solution is obtained, the rank constraint was enforced using a rank reduction technique like randomization or singular value decomposition (SVD) if $\mathrm{rank}(\mathbf{W}_{\mathrm{AB}}) \neq 1$.

Furthermore, the sub-problem in terms of $\mathbf{W}_k$ was presented in (17). This problem solves the optimal weights of the radar transmitter to increase the average secrecy capacity of the setup demonstrated in Fig. 2.

$$\max_{\mathbf{W}_k} \quad \log_2\left(1 + \gamma_{\mathrm{B}}\right) - \log_2\left(1 + \hat{\gamma}_{\mathrm{E}}\right), \tag{17a}$$

$$\text{s.t.} \quad \log_2\left(1 + \frac{\sum_{l=1}^{L} \mathrm{Tr}\left(\mathbf{H}_{l\mathrm{D}} \mathbf{W}_k \mathbf{H}_{l\mathrm{D}}^{\mathrm{H}}\right)}{\sigma_{\mathrm{D}}^2}\right) \geq r_{\mathrm{th}}, \tag{17b}$$

$$\sum_{l=1}^{L} \mathrm{Tr}\left(\mathbf{H}_{l\mathrm{B}} \mathbf{W}_k \mathbf{H}_{l\mathrm{B}}^{\mathrm{H}}\right) + \mathrm{Tr}\left(\mathbf{H}_{\mathrm{CB}} \mathbf{W}_k \mathbf{H}_{\mathrm{CB}}^{\mathrm{H}}\right) = 0, \tag{17c}$$

$$\mathrm{Tr}(\mathbf{W}_k) = 1, \tag{17d}$$

$$\mathrm{rank}(\mathbf{W}_k) = 1. \tag{17e}$$

Equation (17) is an SDP problem. The transformation and proof of the concavity of the objective function in (17) has been relegated to the Appendix. The rank constraint was resolved using the technique described under (16). Hence, a convex equivalent of (17) was obtained and shown in (18).

$$\max_{\mathbf{W}_k} \quad \log_2\left(a - \frac{b}{y1 + y2 + b + \sigma_{\mathrm{E}}^2}\right), \tag{18a}$$

$$\text{s.t.} \quad \log_2\left(1 + \frac{\sum_{l=1}^{L} \mathrm{Tr}\left(\mathbf{H}_{l\mathrm{D}} \mathbf{W}_k \mathbf{H}_{l\mathrm{D}}^{\mathrm{H}}\right)}{\sigma_{\mathrm{D}}^2}\right) \geq r_{\mathrm{th}}, \tag{18b}$$

$$\sum_{l=1}^{L} \mathrm{Tr}\left(\mathbf{H}_{l\mathrm{B}} \mathbf{W}_k \mathbf{H}_{l\mathrm{B}}^{\mathrm{H}}\right) + \mathrm{Tr}\left(\mathbf{H}_{\mathrm{CB}} \mathbf{W}_k \mathbf{H}_{\mathrm{CB}}^{\mathrm{H}}\right) = 0, \tag{18c}$$

$$\mathrm{Tr}(\mathbf{W}_k) = 1, \tag{18d}$$

where $a = 1 + \gamma_{\mathrm{B}}$, $y1 = \sum_{l=1}^{L} \mathrm{Tr}(\mathbf{H}_{l\mathrm{E}} \mathbf{W}_k \mathbf{H}_{l\mathrm{E}}^{\mathrm{H}})$, $y2 = \mathrm{Tr}(\mathbf{H}_{\mathrm{CE}} \mathbf{W}_k \mathbf{H}_{\mathrm{CE}}^{\mathrm{H}})$, $b = \mathrm{Tr}(\mathbf{H}_{\mathrm{AE}} \mathbf{W}_{\mathrm{AB}} \mathbf{H}_{\mathrm{AE}}^{\mathrm{H}})$. We note that (18) can be solved with CVX [23].

In summary, the procedure to solve (14) follows Algorithm 1. We note that m_{max} is the maximum number of iterations. If the iterations terminate at the maximum number, then convergence was not obtained and the solution to the problem fails. However, it was shown in Fig. 3 that Algorithm 1 always converges within a few numbers of simulations.

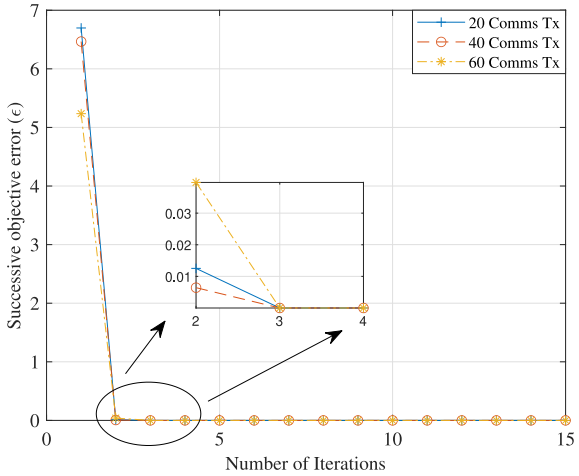

FIGURE 3. Convergence of the sensing Algorithm 1.

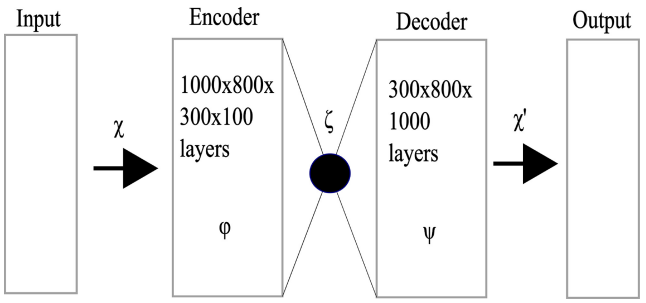

FIGURE 4. Layer interaction of the autoencoder.

C. UNCOOPERATIVE SYSTEMS

When the radar and communications systems are uncooperative, the channel impulse responses are unknown. Hence relying on beamforming weights as an interference mitigation approach is insufficient. This is because nulling the channels as carried out in (4b) and (7b) cannot be performed without knowledge of the channel impulse response. Therefore, to mitigate the cross interference of such radar communication systems, we implement a filter technology using autoencoder as shown in Fig. 4. Autoencoders use feature extraction to learn the variability of multi-dimensional noisy data. The extraction is used to determine the noiseless version of the input data [24]. The noisy data referred to in this work include the desired signals, cross-interference signals and AGWN.

The schematic of the autoencoder network deployed herein was presented in Fig. 4. From Fig. 4, the input and output data were represented as χ and χ' respectively, while ζ gives the data exchanged between the encoder and decoder. ϕ and Ψ are the encoder and decoder activation functions respectively. The activation function refers to the drivers of a group of neurons classified as hidden layers of the autoencoder. The encoder comprises $1000 \times 800 \times 300 \times 100$ hidden layers where the numbers refer to the number of neurons. Similarly, the decoder comprises $300 \times 800 \times 1000$ hidden layers. In artificial neural networks, there are no

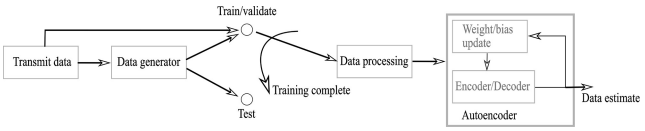

FIGURE 5. Data flow to the autoencoder.

standard methods to accurately predict the optimal number of neurons and hidden layers required for a set of non-linear problems [25]. However, in this paper, the number of neurons and hidden layers used to construct the autoencoder were obtained by a brute pruning method. The pruning method allows for the evaluation of the weights after training a small data set and eliminating neurons with little or no contribution to the learning process.

Each hidden layer of the encoder and decoder were activated with a rectified linear unit (ReLU) function. The neurons of the layers were also assigned a pair of weight and bias to characterise the feature impact ascribed to the neuron. The relation between the output of the autoencoder through the hidden layers of the encoder and decoder sections is given in (19) [24], [25].

$$\chi' = \Psi\big(\mathbf{W}'\phi(\mathbf{W}\chi + \mathbf{b}) + \mathbf{b}'\big). \tag{19}$$

We note that $\{\mathbf{W}, \mathbf{b}\}$ and $\{\mathbf{W}', \mathbf{b}'\}$ are the pair weights and biases for the encoder and decoder parts of the autoencoder respectively. The weights and biases were constantly updated during the training phase to construct the network for feature extraction of the test data.

The deployment of the autoencoder follows two distinct phases - training and testing as depicted in Fig. 5. The training phase allows the network to configure and validate its parameters (weights and biases) using known data. While the testing phases accept unknown data and make predictions based on the configurations obtained during training.

During the training, the network is configured to minimize the reconstruction loss given as

$$\mathcal{L}(\chi, \chi') = ||\chi - \chi'||^2,$$

where $\chi' = \psi(\mathbf{W}'\phi(\mathbf{W}\chi + \mathbf{b}) + \mathbf{b}')$, $\{W, b\}$, $\{W', b'\}$ are the pair weights and biases for the encoder and decoder parts of the autoencoder. ϕ and ψ are the encoder and decoder activation functions respectively.

The neural network is first trained and validated with contextualized pilot data to extract features of the channel response and noise impact. Each snapshot of data comprises 20,000 variations of a communication pilot signal and the radar target reflections. The layers of the autoencoders are activated using rectifier units. During the training phase, 10% of the training data was used for validation. When the training phase is complete, the JCR signals are processed with the trained autoencoder networks at the communication and radar receivers. Since this neural network is domicile at the receivers, an increased number of communication users or radar targets does not affect its functionality.

TABLE 1. Parameter description of the JCR model.

Simulation parameter	Symbol	Value
Number of communication transmit antennas	N_{A}	30
Number of communication receive antennas	N_{B}	4
Number of radar transmit antennas	N_{C}	30
Number of radar receive antennas	N_{D}	4
Carrier frequency (Surveillance)	f_c	2GHz
Distance between antenna elements	d_x	$\frac{\lambda}{2}$
Number of reflecting targets	L	3
Noise power	σ^2_{B} and σ^2_{D}	30dBm
Number of channel realizations		500

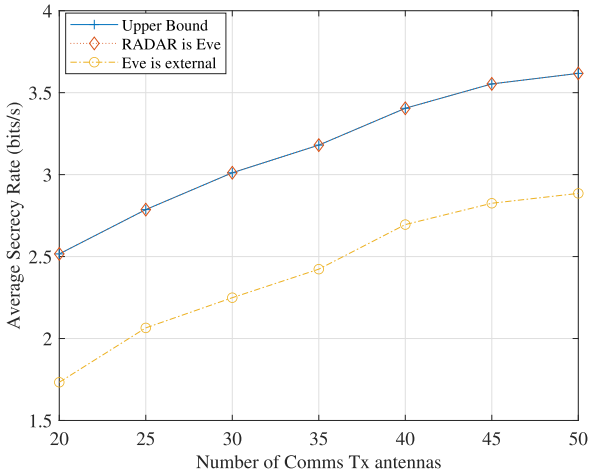

FIGURE 6. PLS comparison with the optimal solution to (4).

IV. RESULTS AND DISCUSSIONS

The performance evaluation of the techniques discussed herein was obtained via MATLAB simulations. The legends in Fig. 6 describe the number of radar antennas and the rate under consideration. In Figs. 9 and 10, the legends describe the number of snapshots used in training the network, whereas 'CRB Null Space Projection' and 'CRB (Original)' presents the null space projection [9] and the Cramer Rao lower bound [26] respectively given known impulse response. The values of other simulation parameters are given in Table 1.

In Fig. 6, the cooperative system analysis of the communication and radar systems developed in Section III-A was presented. Recall that for a cooperative system, the channel information of the radar and communication systems are shared, and thereby effectively considered in the beamforming designs. From (4b) and (7b), the cross interference from both communication and radar systems was suppressed with the choice of the beamforming weights. The effectiveness of the beamforming designs alludes to the observation in Fig. 6 that although the radar receivers are illegitimate listeners of the communication signal, the average secrecy rate was shown to be approximately the same as the rate of the legitimate communication receiver. The rate of the legitimate communication receiver defines the upper bound to the average secrecy rate. In addition, we note that when the eavesdropper is not the radar receiver, thereby existing in an

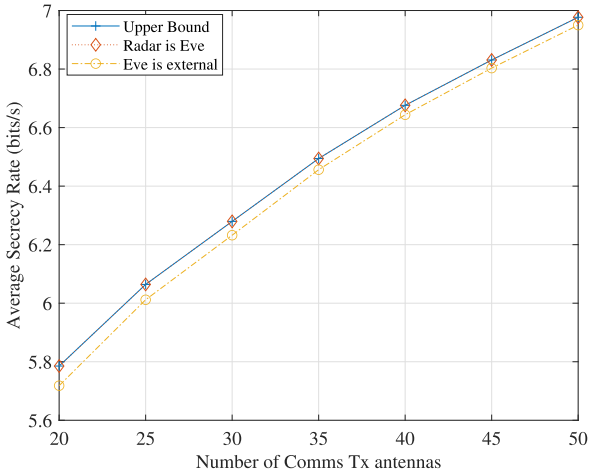

FIGURE 7. PLS comparison with the optimal solution to (13).

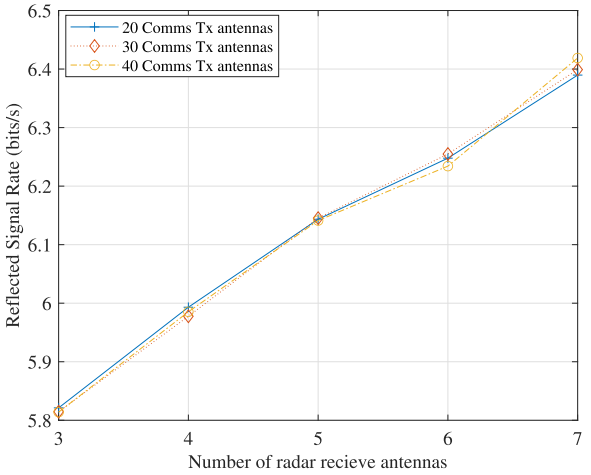

FIGURE 8. Impact of the beamforming design on the radar receiver for $N_A = 30$.

uncertain region, the average secrecy rate becomes smaller. This is because the beamforming designs do not null the external eavesdropper channel since it is unknown. However, even in the external eavesdropper scenario, the secrecy rate is positive and with an increasing number of transmission antennas. The result was expected since the cohabiting signal continues to offer interference at receivers not classified as legitimate. Additionally, from Fig. 6, it was observed that while an increase in the number of communication transmits antennas improves the performance of the systems in terms of transmission rate and average secrecy rate, the number of radar antennas has little/no impact. This is because the interference caused by the radar transmission was effectively removed by the proper design of beamforming weights.

Furthermore, we consider the PLS analysis of the communication/radar cohabiting system when PLS was considered in the design of the transmitter and receiver parameters as shown in Fig. 7. It is clear from Fig. 7 that when the eavesdropper is not the radar receiving antenna, high PLS was obtained. Such high PLS was closer to the maximum rate when compared to the observations in Fig. 6. This further supports the claim that exploring techniques to cancel the interfering signal arising from cohabitation leads to higher PLS.

In addition, we consider the effect of designs of the transmit wireless communication and radar beamforming designs and showed the performance in Fig. 8. It is clear from the figure that only the radar antenna parameters affect the reception rates. By increasing the number of antennas at the radar receiver, the rates of the reflected signals increase. However, changing the number of wireless communication transmitter, do not cause a significant change in the reflected radar rates as observed from both Fig. 8. Although the wireless communication transmission continues to interfere with the radar-reflected signals, the designs of the beamforming weights of the wireless communication ensure that the impact of the interference is negligible.

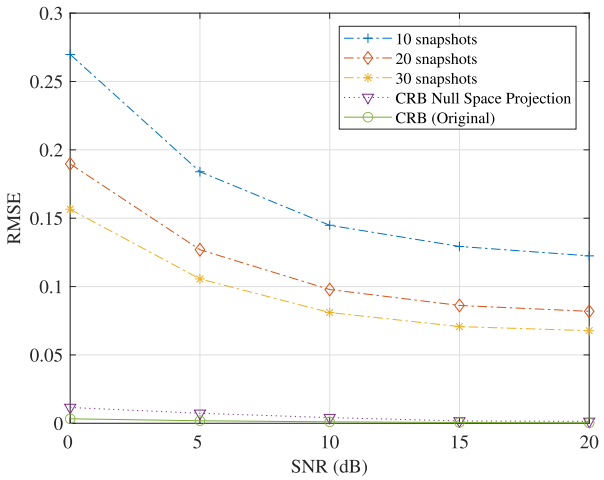

FIGURE 9. RMSE performance graph of test communication signals.

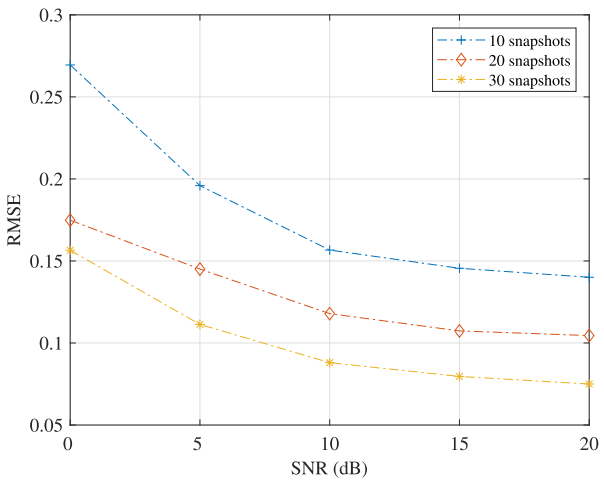

FIGURE 10. RMSE performance graph of test radar reflected signals.

Figures 9 and 10 illustrate the root mean square error (RMSE) of the interference cancelled received signal of the communication and radar signals respectively. For both

figures, a higher signal-to-noise ratio (SNR) presents lower decoding error (in terms of RMSE). By increasing the number of snapshots taken to train the neural network, better performance was observed in both cases respectively. Specifically in Fig. 9, the RMSE values were compared to the performance from the null projection from [9] and the Cramer Rao bound (CRB). We note that the channel response from [9] and CRB was known hence the lower RMSE. It is significant to observe that although better performance was observed with increasing snapshots, it is required that to approach the lower bounds, large snapshots were needed. While this is desired, it places a constraint on the physical device used for training purposes.

V. CONCLUSION

In conclusion, we assert that when full of part channel information was readily available, beamforming design mitigates the interference of radar and communication signals. However, under practical scenarios, where the channel information is usually indeterminate, we investigated a neural network-based approach to filtering interfering and noise signals from the JCR system. We showed that a sizeable chunk of training data guaranteed better interference and noise cancellation when test data were deployed. This invariably leads to efficient cohabitation of the communication and radar systems. Therefore, the interference and noise cancellation approach is applicable when it is infeasible to estimate the channel properties of the JCR system as in real-time applications but where large historic contextualised training data is available. In future, we recommend experimental trials of the proposed interference and noise cancellation system.

APPENDIX

In this Appendix, we show that the objective function in (17) is convex. For clarity, let

$$f(\mathbf{W}_k) = \log_2\left(1+\gamma_{\mathrm{B}}\right) - \log_2\left(1+\hat{\gamma}_{\mathrm{E}}\right).$$

Recall that $\gamma_{\mathrm{B}} = \frac{\mathrm{Tr}(\mathbf{H}_{\mathrm{AB}}\mathbf{W}_{\mathrm{AB}}\mathbf{H}_{\mathrm{AB}}^{\mathrm{H}})}{\sigma_{\mathrm{B}}^2}$ and

$$\hat{\gamma}_{\mathrm{E}} = \frac{\mathrm{Tr}\left(\mathbf{H}_{\mathrm{AE}}\mathbf{W}_{\mathrm{AB}}\mathbf{H}_{\mathrm{AE}}^{\mathrm{H}}\right)}{\sum_{l=1}^{L}\mathrm{Tr}\left(\mathbf{H}_{l\mathrm{E}}\mathbf{W}_k\mathbf{H}_{l\mathrm{E}}^{\mathrm{H}}\right)+\mathrm{Tr}\left(\mathbf{H}_{\mathrm{CE}}\mathbf{W}_k\mathbf{H}_{\mathrm{CE}}^{\mathrm{H}}\right)+\sigma_{\mathrm{E}}^2}.$$

Let $(1+\gamma_{\mathrm{B}}) = a$, $\frac{\mathrm{Tr}(\mathbf{H}_{\mathrm{AE}}\mathbf{W}_{\mathrm{AB}}\mathbf{H}_{\mathrm{AE}}^{\mathrm{H}})}{\sigma_{\mathrm{E}}^2} = b$. For simplification without loss of generality, we assume that $L = 1$. This assumption provides that a single object is reflecting the radar signal to the receivers, i.e., only one radar target. Therefore, by applying [18, eqs. (15)] and the distributive property of matrices, we can write

$$\frac{\mathrm{Tr}\left(\mathbf{H}_{l\mathrm{E}}\mathbf{W}_k\mathbf{H}_{l\mathrm{E}}^{\mathrm{H}}\right)+\mathrm{Tr}\left(\mathbf{H}_{\mathrm{CE}}\mathbf{W}_k\mathbf{H}_{\mathrm{CE}}^{\mathrm{H}}\right)}{\sigma_{\mathrm{E}}^2} = \frac{\mathrm{Tr}\left(\mathbf{W}_k\left(\mathbf{H}_{l\mathrm{E}}^{\mathrm{H}}\mathbf{H}_{l\mathrm{E}}+\mathbf{H}_{\mathrm{CE}}^{\mathrm{H}}\mathbf{H}_{\mathrm{CE}}\right)\right)}{\sigma_{\mathrm{E}}^2}$$

Let $\mathbf{A} = \mathbf{H}_{l\mathrm{E}}^{\mathrm{H}}\mathbf{H}_{l\mathrm{E}}+\mathbf{H}_{\mathrm{CE}}^{\mathrm{H}}\mathbf{H}_{\mathrm{CE}}$ then we can write

$$\begin{aligned} f(\mathbf{W}_k) &= \log_2(a) - \log_2\left(1+\frac{b}{\mathrm{Tr}(\mathbf{W}_k\mathbf{A})+1}\right) \\ &= \log_2\left(\frac{a(\mathrm{Tr}(\mathbf{W}_k\mathbf{A})+1)}{\mathrm{Tr}(\mathbf{W}_k\mathbf{A})+b+1}\right) \\ &= \log_2\left(\frac{a\mathrm{Tr}(\mathbf{W}_k\mathbf{A})+a+a(b+1)-a(b+1))}{\mathrm{Tr}(\mathbf{W}_k\mathbf{A})+b+1}\right) \\ &= \log_2\left(a-\frac{b}{\mathrm{Tr}(\mathbf{W}_k\mathbf{A})+b+1}\right). \end{aligned}$$

We note that $f(\mathbf{W}_k) = h(g(\mathbf{W}_k))$, where $h(.) = \log_2(.)$ and $g(\mathbf{W}_k) = (a-\frac{b}{\mathrm{Tr}(\mathbf{W}_k\mathbf{A})+b+1})$. From the definition, we observe that $h : \mathbf{R} \to \mathbf{R}$ and $g : \mathbf{R}^n \to \mathbf{R}$, we can apply the deduction of scalar composition given in [27, eq. (3.10)] that states that if h is concave and nondecreasing and g is concave, then f is concave (Proof is available in [27]). Since $h(.) = \log_2(.)$ is concave and nondecreasing, we show that $g(\mathbf{W}_k)$ is concave.

In general, if the Hessian or second derivative of the function $\nabla^2 g(\mathbf{W}_k)$ exists, then its concavity defined by [27] is $\nabla^2 g(\mathbf{W}_k) \preceq 0$.

By expanding the second derivation of $g(\mathbf{W}_k)$, we have that

$$\nabla^2 g(\mathbf{W}_k) = \frac{-2b(\mathbf{A}^{\mathrm{H}})^2}{(1+b+\mathrm{Tr}(\mathbf{W}_k\mathbf{A}))^3}.$$

We then show that $\nabla^2 g(\mathbf{W}_k) \preceq 0$ by

$$\begin{aligned} \mathbf{v}^{\mathrm{T}}\nabla^2 g(\mathbf{W}_k)\mathbf{v} &= \frac{-\mathbf{v}^{\mathrm{T}}2b(\mathbf{A}^{\mathrm{H}})^2\mathbf{v}}{(1+b+\mathrm{Tr}(\mathbf{W}_k\mathbf{A}))^3}, \\ &= \frac{-2b}{(1+b+\mathrm{Tr}(\mathbf{W}_k\mathbf{A}))^3}\mathbf{v}^{\mathrm{T}}\mathbf{A}^{\mathrm{H}}\mathbf{A}\mathbf{v}, \\ &= \frac{-2b}{(1+b+\mathrm{Tr}(\mathbf{W}_k\mathbf{A}))^3}|\mathbf{A}\mathbf{v}|^2, \end{aligned}$$

By applying Cauchy-Schwarz inequality,

$$\mathbf{v}^{\mathrm{T}}\nabla^2 g(\mathbf{W}_k)\mathbf{v} = \frac{-2b}{(1+b+\mathrm{Tr}(\mathbf{W}_k\mathbf{A}))^3}\|\mathbf{A}\|^2|\mathbf{v}|^2 \le 0,$$

for all vectors, $\mathbf{v}$. Since $g(\mathbf{W}_k)$ is concave and $h(.)$ is concave nondecreasing, it, therefore, follows that $f(\mathbf{W}_k)$ is concave. This assertion also follows from [27, Example 3.13] that if $g(x)$ is concave and positive, then $\log g(x)$ is also concave. While we have presented the concavity of $g(\mathbf{W}_k)$, we note that it is required from (12) that the legitimately received signals should be better than the eavesdropped, hence, $g(\mathbf{W}_k)$ is always positive. As a consequence, the SNR of $a \ge 0$, $b \ge 0$ and $1+b+\mathrm{Tr}(\mathbf{W}_k\mathbf{A}) \ge 0$.

REFERENCES

[1] A. Martone and M. Amin, "A view on radar and communication systems coexistence and dual functionality in the era of spectrum sensing," *Digit. Signal Process.*, vol. 119, 2021, Art. no. 103135. [Online]. Available: https://www.sciencedirect.com/science/article/pii/S1051200421001743

[2] J. Lundén, "Spectrum sensing for cognitive radio and radar systems," Ph.D. dissertation, Dept. Signal Process. Acoustics, Helsinki Univ. Technol., Espoo, Finland, 2009.

[3] A. Nasser, A. H. Hassan, J. A, haaya, A. Chaaya, and K. C. Yao, "Spectrum sensing for cognitive radio: Recent advances and future challenge," *Sensors*, vol. 21, no. 7, p. 2408, 2021.
[4] S. Mazahir, S. Ahmed, and M.-S. Alouini, "A survey on joint communication-radar systems," *Front. Commun. Net.*, vol. 1, p. 9, Feb. 2021, [Online]. Available: https://www.frontiersin.org/article/10.3389/frcmn.2020.619483
[5] F. Liu, C. Masouros, A. P. Petropulu, H. Griffiths, and L. Hanzo, "Joint radar and communication design: Applications, state-of-the-art, and the road ahead," *IEEE Trans. Commun.*, vol. 68, no. 6, pp. 3834–3862, Jun. 2020.
[6] J. A. Zhang et al., "An overview of signal processing techniques for joint communication and radar sensing," *IEEE J. Select. Topics Signal Process.*, vol. 15, no. 6, pp. 1295–1315, Nov. 2021.
[7] R. Thomä, T. Dallmann, S. Jovanoska, P. Knott, and A. Schmeink, "Joint communication and radar sensing: An overview," in *Proc. 15th Eur. Conf. Antennas Propagat. (EuCAP)*, 2021, pp. 1–5.
[8] H. Li, "Inseparable waveform synthesis in joint communications and radar via spatial-frequency spectrum," in *Proc. IEEE Global Commun. Conf. (GLOBECOM)*, 2021.
[9] S. Sodagari, A. Khawar, T. C. Clancy, and R. McGwier, "A projection based approach for radar and Telecommun. Syst. coexistence," in *Proc. IEEE Global Commun. Conf. (GLOBECOM)*, 2012, pp. 5010–5014.
[10] A. Hassanien, B. Himed, and M. G. Amin, "Transmit/receive beamforming design for joint radar and communication systems," in *Proc. IEEE Radar Conf. (RadarConf18)*, 2018, pp. 1481–1486.
[11] F. Liu, C. Masouros, A. Li, H. Sun, and L. Hanzo, "MU-MIMO communications with MIMO radar: From co-existence to joint transmission," *IEEE Trans. Wireless Commun.*, vol. 17, no. 4, pp. 2755–2770, Apr. 2018.
[12] N. Su, F. Liu, and C. Masouros, "Enhancing the physical layer security of dual-functional radar communication systems," in *Proc. IEEE Global Commun. Conf. (GLOBECOM)*, 2019, pp. 1–6.
[13] A. Hassanien, M. G. Amin, Y. D. Zhang, and F. Ahmad, "Dual-function radar-communications: Information embedding using Sidelobe control and waveform diversity," *IEEE Trans. Signal Process.*, vol. 64, no. 8, pp. 2168–2181, Apr. 2016.
[14] A. N. Pineda, L. U. Aragonés, J. R. F. del Castillo Díez, and M. Ángel Patricio Guisado, "Radar tracking system using contextual information on a neural network architecture in air combat maneuvering," *Int. J. Distrib. Sensor Net.*, vol. 9, no. 8, pp. 1–11, 2013.
[15] A. Li, Q. Wu, and R. Zhang, "UAV-enabled cooperative jamming for improving secrecy of ground wiretap channel," *IEEE Wireless Commun. Lett.*, vol. 8, no. 1, pp. 181–184, Feb. 2019.
[16] X. Zhou, Q. Wu, S. Yan, F. Shu, and J. Li, "UAV-enabled secure communications: Joint trajectory and transmit power optimization," *IEEE Trans. Veh. Technol.*, vol. 68, no. 4, pp. 4069–4073, Apr. 2019.
[17] C. O. Nnamani, M. R. A. Khandaker, and M. Sellathurai, "Secure data collection via UAV-carried IRS," *ICT Exp.* vol. 9, no. 4, pp. 706–713, 2023.
[18] K. B. Petersen and M. S. Pedersen, "The matrix cookbook," Nov. 2012, version 20121115, [Online]. Available: http://localhost/pubdb/p.php?3274
[19] M. Grant and S. Boyd. "CVX: MATLAB software for disciplined convex programming; version 2.1." Mar. 2014. [Online]. Available: http://cvxr.com/cvx
[20] C. O. Nnamani, M. R. Khandaker, and M. Sellathurai, "Secrecy rate Maximization with gridded UAV swarm jamming for passive eavesdropping," in *Proc. IEEE Global Commun. Conf. (GLOBECOM)*, 2021, pp. 1–6.
[21] P. K. Gopala, L. Lai, and H. E. Gamal, "On the secrecy capacity of fading channels," *IEEE Trans. Inf. Theory*, vol. 54, no. 10, pp. 4687–4698, Oct. 2008.
[22] C. O. Nnamani, M. R. A. Khandaker, and M. Sellathurai, "UAV-aided jamming for secure ground communication with unknown eavesdropper location," *IEEE Access*, vol. 8, pp. 72881–72892, 2020.
[23] M. Grant and S. Boyd, "Recent advances in learning and control," in *Graph Implementations For Nonsmooth Convex Programs* (Lecture Notes in Control and Information Sciences). Berlin, Germany: Springer-Verlag, Mar. 2008, pp. 95–110.
[24] G. K. Papageorgiou and M. Sellathurai, "Fast direction-of-arrival estimation of multiple targets using deep learning and sparse arrays," in *Proc. Int. Conf. Acoust., Speech, Signal Process. (ICASSP)*, 2020, pp. 4632–4636.
[25] I. Goodfellow, Y. Bengio, and A. Courville, *Deep Learning*. Cambridge, MA, USA: MIT Press, 2016. [Online]. Available: http://www.deeplearningbook.org
[26] J. Li and P. Stoica, *MIMO Radar Signal Processing*. Hoboken, NJ, USA: Wiley, 2008.
[27] S. Boyd and L. Vandenberghe, "*Convex Optimization*." Cambridge, U.K.: Cambridge Univ. Press, 2004.

CHRISTANTUS OBINNA NNAMANI (Member, IEEE) received the B.Eng. degree in electronic engineering and the M.Eng. and Ph.D. degrees in electronic engineering (Telecommunications) from the University of Nigeria Nsukka, in 2011, 2015, and 2021, respectively, and the second Ph.D. from the School of Engineering and Physical Sciences, Heriot-Watt University, Edinburgh, U.K., in 2022. He is a Research Fellow with Cranfield University investigating projects relating to U.K. Future Flights. He is an experienced researcher with ten years of career experience within the university and research groups. His research interests include PLS, UAV, UTM, ATM, NGN, network security, resource allocation, simulation, and modeling. He has authored and coauthored several academic papers and proceedings. He is a member of several engineering associations, such as the European Association for Signal Processing, the Council for the Regulation of Engineering in Nigeria, and the Nigerian Society of Engineers. He is also a member of the review panel for the IEEE WIRELESS COMMUNICATION LETTERS, IEEE TRANSACTIONS ON VEHICULAR TECHNOLOGY, IEEE COMMUNICATION LETTERS, and *Cogent Engineering* (Elsevier). He is an Associate Fellow of HEA and a member of IET.

MATHINI SELLATHURAI (Senior Member, IEEE) is a Full Professor of Signal Processing and Intelligent Systems, Heriot-Watt University, Edinburgh, U.K. In her 20-year research on Signal Processing for Communications, she has made seminal contributions on MIMO wireless systems. She has published over 200 IEEE entries, given invited talks and has written a book and several book chapters in topics related to this project. She received the IEEE Communication Society Fred W. Ellersick Best Paper Award in 2005, Industry Canada Public Service Awards for contributions in science and technology in 2005, and the Best Ph.D. Thesis Medal from NSERC Canada in 2002. She is also a member for IEEE SPCOM Technical Strategy Committee from 2014 to 2018 and an Editor for IEEE TRANSACTIONS ON SIGNAL PROCESSING from 2009 to 2014 and from 2015 to 2018. She was also the General Co-Chair of IEEE SPAWC2016 in Edinburgh. She is a Fellow of HEA.